Detection of Root Knot Nematodes in Microscopy Images

Faroq AL-Tam[1,2], António dos Anjos[3,4], Stephane Bellafiore[5,6] and Hamid Reza Shahbazkia[1,7]
[1]*Department of Electronic and Informatics Engineering, University of Algarve, Faro, Portugal*
[2]*Faculty of Computer Science and Information Technology, University of Thamar, Dhamar, Yemen*
[3]*ISMAT, Portimão, Portugal*
[4]*CCMAR-CIMAR Laboratório Associado, University of Algarve, 8005-139 Faro, Portugal*
[5]*RPB, IRD Montpellier, France*
[6]*LMI RICE, Hanoi, Vietnam*
[7]*MIVEGEC, IRD Montpellier, France*

Keywords: Root Knot Nematodes, Vessel-like Detection, Illumination Correction, Thining, Mathematical Morphology.

Abstract: Object detection in microscopy image is essential for further analysis in many applications. However, images are not always easy to analyze due to uneven illumination and noise. In addition, objects may appear merged together with debris. This work presents a method for detecting rice root knot nematodes in microscopy images. The problem involves four subproblems which are dealt with separately. The uneven illumination is corrected via polynomial fitting. The nematodes are then highlighted using mathematical morphology. A binary image is obtained and the microscope lines are removed. Finally, the detected nematodes are counted after thresholding the non-nematode particles. The results obtained from the performed tests show that this is a reliable and effective method when compared to manual counting.

1 INTRODUCTION

Root Knot Nematodes (RKN) are plant parasitic microscopic animals responsible for a farm loss up to $157 billion every year (Abad et al., 2008). All efficient pesticides on RKN are not only toxic to humans but also to the environment and have been banned recently in most countries (M.B.T.O.Committee, 2010). Pest management required an alternative. One promising strategy is to find resistant plants that could be crossed with interesting farmer crops to give a resistant cultivar. However, breeding programs need the ability of evaluating the plants' resistance to the nematode. To assess the resistance of a germplasm to RKN, one should be able to exhaustively count the offsprings' number after a complete nematode life cycle. But for microscopic parasites such as nematodes, the process can be extremely time consuming and error prone. Counting objects under microscope for a single plant takes around 15 to 30 minutes depending on the quantity of parasites. Moreover, the plant breeder has to conscientiously observe the sample under microscope to specifically count the number of parasites. During the nematode sampling, several soil and plant compounds are collected and can be misinterpreted as nematodes. To date, to our knowledge, no software has been developed to assist plant breeders in their resistance evaluation. Developing image processing methods to allow the automation or semi automation of the counting process will drastically influence the precision and speed of these kind of experiments and will allow faster experiment setups and better results. This work describes an automatic method for analyzing RKN in microscopy images.

2 THE PROPOSED APPROACH

This section addresses the technical details of the problem and the proposed approach. In essence, four different subproblems will be dealt with and solved. These are:

1. Illumination correction.
2. Foreground detection.
3. Microscope lines suppression.
4. Nematode identification.

AL-Tam F., dos Anjos A., Bellafiore S. and Shahbazkia H..
Detection of Root Knot Nematodes in Microscopy Images.
DOI: 10.5220/0005209000760081
In *Proceedings of the International Conference on Bioimaging* (BIOIMAGING-2015), pages 76-81
ISBN: 978-989-758-072-7

2.1 Illumination Correction

Due to the variations in the light when acquiring the images, illumination bias is recurrent in microscopy imaging. In this work, the input images are contaminated by an uneven illumination field (Figure 1), which has to be removed beforehand. To this end, the input image is modeled by the multiplicative model as (Young, 2001; Gonzalez and Woods, 2002):

$$S = T.B + \varepsilon \tag{1}$$

Where the matrices $S \in \mathbb{R}^{m\times n}, T \in \mathbb{R}^{m\times n}$, and $B \in \mathbb{R}^{m\times n}$, are the observed image, the true image, and the bias field, respectively. "." is the Hadamard element-wise product, and $\varepsilon \in \mathbb{R}^{m\times n}$ is additive noise. Obviously, (1) is an inverse ill-posed problem, because the number of equations is lower than the number of unknowns.

The input image can be enhanced by suppressing the noise, simplifying Equation (1). The type of the noise can be estimated by examining the distribution of a clear (background only) region in the image. Figure 2b shows a clear Gaussian distribution as being the histogram of the background image. For that reason, the image is preprocessed by convolving it with a Gaussian low pass filter with a kernel size k.

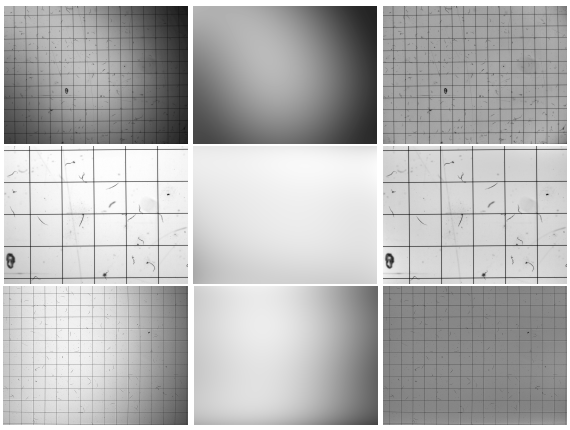

Figure 1: Illumination correction. Left: the input image, middle: the estimated bias B, and right: the recovered image T.

With the noise being removed, ε can be ignored and (1) can be rewritten as:

$$\log(S) = \log(T) + \log(B) \tag{2}$$

In (2), estimating B can be done in many different ways. A comprehensive review can be found in (Hou, 2006; Vovk et al., 2007). Among these approaches, surface fitting is suitable for this kind of images. This type of images contain thin structures, therefore, a proper 2-D smooth function can accurately model B

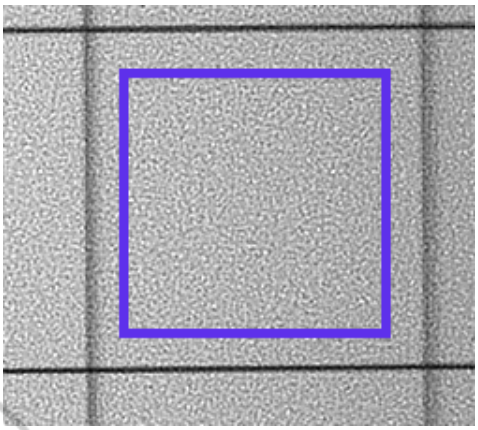

(a) A background region bounded by a rectangle.

(b) Respective intensity distribution

Figure 2: Identification of the noise type.

without including the objects in the estimated field. In addition, estimating B by using a 2-D smooth function reflects the main property of the illumination field, *i.e.* B is assumed to be a slowly varying field.

B is modeled by using a bivariate polynomial of degree d, where each pixel of $B(x,y)$ is calculated as:

$$B(x,y;\vec{\theta},d) = \sum_{i=0}^{i=d}\sum_{j=0}^{j=i} \theta_{i,j} x^{i-j} y^{j} \tag{3}$$

which, in matrix form, can be rewritten as:

$$B = V\vec{\theta} = \begin{bmatrix} 1 & x_1 & y_1 & \dots & x_1^{i-j}y_1^j \\ \vdots & \vdots & \vdots & \ddots & \vdots \\ 1 & x_r & y_r & \dots & x_r^{i-j}y_r^j \end{bmatrix} \times \begin{bmatrix} \theta_{0,0} \\ \theta_{1,0} \\ \theta_{1,1} \\ \vdots \\ \theta_{d,d} \end{bmatrix} \tag{4}$$

with $r = mn$. The problem of calculating B from (2), boils down to a least squares problem of estimating the vector of parameters $\vec{\theta}$ as:

$$\arg\min_{\vec{\theta}} \frac{1}{2}\|V\vec{\theta} - \vec{s}\|_2^2 \tag{5}$$

where $\vec{s}$ is a vector created by concatenating the columns of S. $\vec{\theta}$ can be therefore found by the normal equations as:

$$\vec{\theta} = (V^\top V)^{-1} V^\top \vec{s} \tag{6}$$

Examples of applying the illumination correction are shown in Figure 1.

2.2 Foreground Detection

In some situations, general thresholding approaches, like iso-data (Trussell, 1978), Otsu (Otsu, 1975), and local-mean (Fisher R., 1996) may be suitable for detecting the foreground. However, such methods are general, in the sense that they statistically estimate a threshold that separates two classes in the image data. In other words, they use zero knowledge about the shape of the objects to be detected. These methods even if success to segment the image, they will detect all objects regardless of their shape. In this work, only elongated objects are targeted, therefore, the detection of the nematodes is two-fold. First, thin structures are highlighted. Second, the resulting image is segmented in order to obtain a binary version.

2.2.1 Detection of Thin Structures

The detection of thin and vessel-like structures is a popular problem, especially in the medical and microscopy image analysis community. For this purpose, different approaches have been developed. Examples include, Frangi's method (Frangi et al., 1998), differential geometry (Steger, 1998), matched filters (Chaudhuri et al., 1989), mathematical morphology (MM) (Zana and Klein, 2001), and tracing methods (Yim et al., 2000; Meijering et al., 2004). An approach using mathematical morphology (MM) (Figueiredo and Leitao, 1995) is chosen due to two reasons. First, most of the other methods have responses at the object's edges, which is not desirable. Second, MM is computationally efficient.

In MM the input image can be looked at as a topographic surface. A nematode can be seen as a narrow continuous plateau with minima spanning its medial line. Here the input image is grayscale with dark objects and light background, and the structuring elements (SE) is flat. A great advantage in MM is that almost all filters are made of two basic building blocks: erosion and dilation (Serra, 1983). The grayscale flat dilation of the image T by the structuring element f is defined as:

$$T \oplus f = \max_{a,b \in f} T(x+a, y+b) \tag{7}$$

Similarly, the flat erosion is defined as:

$$T \ominus f = \min_{a,b \in f} T(x+a, y+b) \tag{8}$$

These two operators are very common and easy to implement as they can be conceived as minimum (for erosion) and maximum (for dilation) filters. Inside a region defined by the geometry of the f (*e.g.* a disk), each pixel of the image is replaced by either the maximum or the minimum neighbor according to the operator type (Figueiredo and Leitao, 1995).

Using these two basic operators, additional filters can be built. Another two popular operators are *open* and *close*. Opening is defined as the erosion followed by dilation:

$$T \circ f = (T \ominus f) \oplus f \tag{9}$$

Likewise, mathematical closing is defined as dilation of erosion:

$$T \bullet f = (T \oplus f) \ominus f \tag{10}$$

For detecting elevations, two specialized operators can be used: top-hat and bottom-hat transforms. A top-hat transform is defined as the difference between the image and an opened version of itself.

$$\tau_{\text{top}}(T, f) = T - (T \circ f) \tag{11}$$

The bottom-hat transform is the difference between the image and a closed version.

$$\tau_{\text{bottom}}(T, f) = T - (T \bullet f) \tag{12}$$

Due to the nice property of the top/bottom-hat transforms of highlighting specific features, they were used in many vessel-like structure detection methods *e.g.* (Zana and Klein, 2001; Mendonça and Campilho, 2006). When an appropriate radius of f is selected, the foreground pixels can be highlighted and the background artifacts can be reduced. Given a flat disk structuring element f, with radius ϑ. The recovered image T is transformed by the bottom-hat operator as in (12). The results of detecting the foreground are shown in Figure 3.

2.2.2 Segmentation

To threshold the response of the bottom-hat transform, let μ be the mean of the image $\tau_{\text{bottom}}(T, f)$. The binary image is obtained as:

$$T_{\text{binary}} = \begin{cases} 255 & \text{if } \tau_{\text{bottom}}(T, f) \leq \mu \\ 0 & \text{otherwise} \end{cases} \tag{13}$$

The result of segmentation is shown in Figure 3.

2.3 Microscope Lines Suppression

With the presence of the microscope lines, it is very difficult to detect the intended objects. The nematode counting cells are provided with carved microscope lines offering the investigator access to a precise volume unit (here, the number of nematodes per

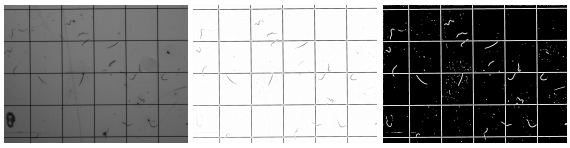

Figure 3: Detection of the nematodes using the bottom-hat transform. Left: a sample image. Middle: the response of the bottom-hat transform of a disk structuring element with radius 5. Right: the resulting binary image.

volume unit). In other words, a counting chamber needs to have these lines to define a volume unit, and nematologists count particles with these lines. However those microscope lines cannot be removed by the investigator as this would modify the volume unit and thereby lose precision. Furthermore, these lines have approximately the same width as the nematodes, which makes the detection task even harder. The removal of the lines is not trivial, because there are intersections between them and the nematodes. Therefore, there has to be a reconnecting approach for nematodes being split.

In order to remove the lines, the Euclidean distance map T_{EDM} (Meijster et al., 2002) and the skeleton T_{skeleton} (Zhang and Suen, 1984) of T_{binary} are calculated. Before removing a line, it is important to know its width. Let a connected component in T_{binary} be denoted by the set of points P. Let $\text{SKELETON}(P) \subseteq P$ be the set of skeleton points of the component P. As these lines correspond to the maximum connected component ($P_{\max}$) in T_{binary}, the radius ρ of the lines is calculated as:

$$\rho(P_{\max}) = \frac{1}{z}\sum_{i=1}^{z} \text{EDM}(p_i), \quad \forall p \in \text{SKELETON}(P_{\max}) \tag{14}$$

where z is the size of $\text{SKELETON}(P_{\max})$.

As the lines are only horizontal and vertical, the skeleton image is convolved by these line detection kernels:

$$h_{\text{horizontal}} = \begin{bmatrix} -1 & -1 & -1 \\ 2 & 2 & 2 \\ -1 & -1 & -1 \end{bmatrix} \tag{15}$$

$$h_{\text{vertical}} = \begin{bmatrix} -1 & 2 & -1 \\ -1 & 2 & -1 \\ -1 & 2 & -1 \end{bmatrix} \tag{16}$$

In the beginning, the skeleton image T_{skeleton} is convolved by the $h_{\text{horizontal}}$ in order to detect the horizontal lines. The region of radius $\rho(P_{\max})$ centered at each one of these lines is suppressed all the way along each line. In order to avoid removing the nematodes that are horizontal, a length threshold ℓ is used to remove any horizontal line with length $\geq \ell$. The same process is repeated with h_{vertical} to detect and suppress the vertical lines. The result of this process is an image without lines T_{clean} (Figure 4).

2.4 Nematodes Identification

During the suppression of the lines, some nematodes are being split. They are rejoined by using a search approach. The detected horizontal lines from T_{skeleton} are scanned against the T_{binary} by passing a vertical line of length $2 * \rho(P_{\max}) + c$ at each point of the horizontal line. Where c is a small integer (*e.g.* 2). If all the points of this small vertical line belong to the foreground of T_{binary}, foreground pixels (*i.e.* 255) are added in the position of this vertical line to the T_{clean} image. The same process is adapted for the vertical lines detected in T_{skeleton}, but using a small horizontal line with the length $2 * \rho(P_{\max}) + c$ as well. The result is an image with the unsplit detected nematodes. In order to filter out the detected debris, the medial axis of each detected object is cleaned by removing skeleton branches of length $\leq 2 * \rho(P_{\max})$ (*i.e.* to smooth the skeleton). This helps to establish a thresholding approach based on the length of the medial axis to differentiate nematodes from other objects. Therefore, among the detected objects, only the ones with length $\geq u$ are identified as nematodes. The accuracy of the proposed method was computed by comparing the number of detected nematodes to the number of nematodes existing in a ground truth.

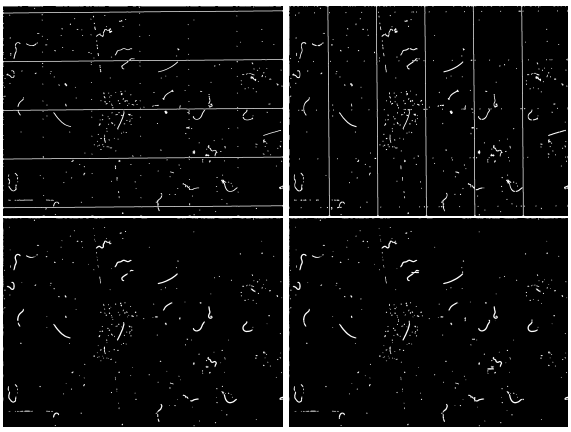

Figure 4: Line detection and suppression. Top row: detecting the horizontal and vertical lines. Bottom row: rejoining the splitted nematodes.

3 RESULTS

To evaluate the described method, a set of 12 grayscale nematode images were used. Each image size is 2048×1536. The method was compared to a

ground truth (GT) of manually counted nematodes. These results are shown in Table 1. The parameters used in this test are shown in Table 2. The detected (Det.) nematodes were evaluated in terms of True Positive (TP), False Positive (FP), False Negative (FN), Positive Predictive Value (PPV) $\frac{TP}{TP+FP}$, and Recall $\frac{TP}{TP+FN}$.

Table 1: Nematode detection results of 12 samples.

#	GT	Det.	TP	FP	FN	PPV	Recall
1	71	66	66	0	5	1.00	0.93
2	75	87	70	17	5	0.80	0.93
3	45	62	45	17	0	0.73	1.00
4	38	42	34	8	4	0.81	0.89
5	33	37	28	9	5	0.76	0.85
6	32	35	30	5	2	0.86	0.94
7	15	17	14	3	1	0.82	0.93
8	21	26	19	7	2	0.73	0.90
9	45	40	36	4	9	0.90	0.80
10	66	59	57	2	9	0.97	0.86
11	39	42	36	6	3	0.86	0.92
12	36	36	36	0	0	1.00	1.00

Table 2: The parameters used (measured in pixels).

Parameter	Description	Value
k	Gaussian kernel radius	3
ℓ	Min. length of a line	$0.3m$
ϑ	Bottom hat transform radius	5
u	Min. length of a nematode	30

The averages of PPV and Recall where ≈ 0.85 and ≈ 0.91, respectively. The FN is low which indicating that the proposed approach performed a good detection. Most of the time the missed nematodes were almost hidden by the microscope lines or partially visible (Figure 5). However, in some cases, there were nematode-like artifacts which increased the number of FP. An example of this kind of non-desirable artifacts is shown in Figure 6. Overall, the method looks very promising and shows reliable results, especially, when it comes to images that do not contain unwanted nematode-like artifacts (Figure 7).

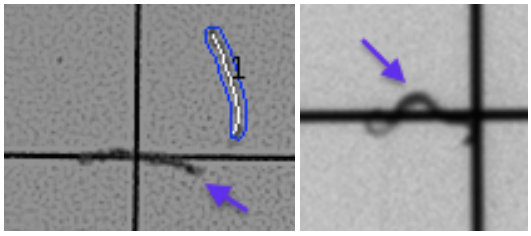

Figure 5: Examples of missed nematodes due to partial visibility (pointed by the arrow).

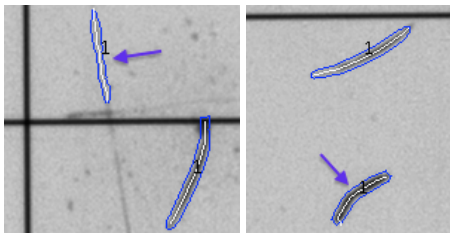

Figure 6: Nematode-like objects (pointed by the arrow).

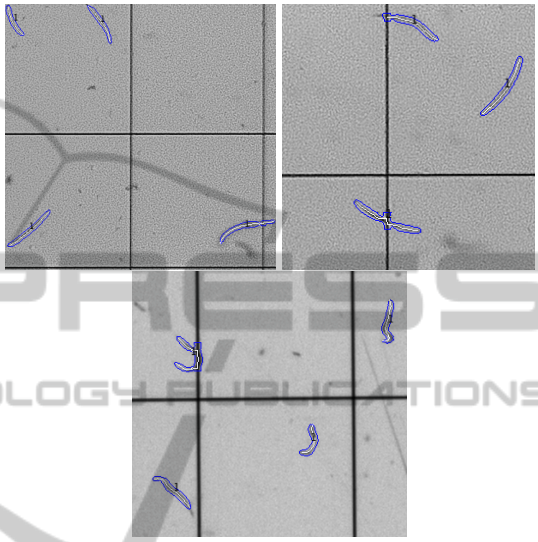

Figure 7: Examples of nematodes detected by the proposed approach.

4 CONCLUSION

A method for Root Knot Nematode detection in microscopy images was presented. The input images suffered from uneven illumination and noise contamination. The noise was suppressed by a Gaussian filter and, then, the illumination was corrected by 2-D polynomial fitting. The mathematical morphology bottom-hat transform is used afterwards to highlight the nematodes. A binary image is obtained by thresholding the response of the bottom-hat. Two filters were used to remove the microscope lines from the binary image. Nematodes being split due to the lines' suppression were merged by a search method. The final quantification results were collected based on a length threshold of the detected object medial axis. The experimental results showed a reliable detection when comparing the method to a manually created ground truth. To evaluate the offsprings' number, classical counting techniques require the presence of one or several researchers in front of their microscope all day long. Mistakes are bound to occur, leading to a misevaluation of the offsprings' number. To bypass this artifact the only solution is to increase the sam-

ple number to obtain statistical significance. However, by doing so, the evaluation time significantly increases. As most laboratories can generate images with a camera linked to a microscope, we believe that our method can be easily extended to their structures offering a fast and reproducible technique. This approach will make way for the development of a platform allowing high throughput selection of plant resistant cultivars. Moreover, beside the direct interest of breeders to this kind of tool, our approach could also be of interest to other biological fields. Indeed, it is possible to measure the number of nematodes per volume unit but also to assess the size of each nematode providing access to traits that could be very informative to ecology studies.

ACKNOWLEDGEMENTS

This work was partially financed by SPIRALE and MENERGEP (GRiSP) projects, IRD Montpellier France. We also acknowledge the INFECTOPOL SUD Marseille France for granting the cooperation.

REFERENCES

Abad, P., Gouzy, J., Aury, J.-M., Castagnone-Sereno, P., Danchin, E. G., Deleury, E., Perfus-Barbeoch, L., Anthouard, V., Artiguenave, F., Blok, V. C., et al. (2008). Genome sequence of the metazoan plant-parasitic nematode meloidogyne incognita. *Nature biotechnology*, 26(8):909–915.

Chaudhuri, S., Chatterjee, S., Katz, N., Nelson, M., and Goldbaum, M. (1989). Detection of blood vessels in retinal images using two-dimensional matched filters. *Medical Imaging, IEEE Transactions on*, 8(3):263–269.

Figueiredo, M. A. and Leitao, J. M. (1995). A nonsmoothing approach to the estimation of vessel contours in angiograms. *Medical Imaging, IEEE Transactions on*, 14(1):162–172.

Fisher R., Perkins S., W. A. . W. E. (1996.). *Hypermedia Image Processing Reference*. J. Wiley & Sons Publishing.

Frangi, A. F., Niessen, W. J., Vincken, K. L., and Viergever, M. A. (1998). Multiscale vessel enhancement filtering. In *Medical Image Computing and Computer-Assisted Interventation - MICCAI 98*, pages 130–137. Springer.

Gonzalez, R. C. and Woods, R. E. (2002). *Digital Image Processing, 2-nd Edition*. Prentice Hall.

Hou, Z. (2006). A review on mr image intensity inhomogeneity correction. *International Journal of Biomedical Imaging*, 2006.

M.B.T.O.Committee (2010). 2010 report of the methyl bromide technical options committee 2010 assessment. Technical report, Nairobi, United Nations Environment Program (UNEP).

Meijering, E., Jacob, M., Sarria, J.-C., Steiner, P., Hirling, H., and Unser, M. (2004). Design and validation of a tool for neurite tracing and analysis in fluorescence microscopy images. *Cytometry Part A*, 58(2):167–176.

Meijster, A., Roerdink, J. B., and Hesselink, W. H. (2002). A general algorithm for computing distance transforms in linear time. In *Mathematical Morphology and its applications to image and signal processing*, pages 331–340. Springer.

Mendonça, A. M. and Campilho, A. (2006). Segmentation of retinal blood vessels by combining the detection of centerlines and morphological reconstruction. *Medical Imaging, IEEE Transactions on*, 25(9):1200–1213.

Otsu, N. (1975). A threshold selection method from gray-level histograms. *Automatica*, 11(285-296):23–27.

Serra, J. (1983). Image analysis and mathematical morphology.

Steger, C. (1998). An unbiased detector of curvilinear structures. *Pattern Analysis and Machine Intelligence, IEEE Transactions on*, 20(2):113–125.

Trussell, H. J. (1978). Picture thresholding using an iterative selection method. *Systems, Man and Cybernetics, IEEE Transactions on*, 8(8):630–632.

Vovk, U., Pernus, F., and Likar, B. (2007). A review of methods for correction of intensity inhomogeneity in mri. *Medical Imaging, IEEE Transactions on*, 26(3):405–421.

Yim, P. J., Choyke, P. L., and Summers, R. M. (2000). Gray-scale skeletonization of small vessels in magnetic resonance angiography. *Medical Imaging, IEEE Transactions on*, 19(6):568–576.

Young, I. T. (2001). *Shading Correction: Compensation for Illumination and Sensor Inhomogeneities*. John Wiley & Sons, Inc.

Zana, F. and Klein, J.-C. (2001). Segmentation of vessel-like patterns using mathematical morphology and curvature evaluation. *Image Processing, IEEE Transactions on*, 10(7):1010–1019.

Zhang, T. Y. and Suen, C. Y. (1984). A fast parallel algorithm for thinning digital patterns. *Commun. ACM*, 27(3):236–239.